DEVELOPMENT OF NANO *IN SITU* GELS OF BEVACIZUMAB FOR THE TREATMENT OF OCULAR ANGIOGENESIS: *IN VITRO* ASSESSMENT OF ANTI-ANGIOGENESIS ACTIVITY AND MOLECULAR DOCKING ANALYSIS

SOUMYA NARAYANA* (ID), MOHAMMED GULZAR AHMED (ID), ARFA NASRINE (ID)

Department of Pharmaceutics, Yenepoya Pharmacy College and Research Centre, Yenepoya (Deemed to be University), Naringana-575023, Mangaluru, Karnataka, India
*Corresponding author: Soumya Narayana and Mohammed Gulzar Ahmed; *Email: kalikollur123@gmail.com

ABSTRACT

Objective: The present investigation aims to develop nano in situ gels of bevacizumab and evaluate their safety and efficacy.

Methods: Nanoparticles were designed using the desolvation and double emulsion solvent evaporation technique. The hen's egg test: chorioallantoic membrane (HET-CAM) assay was adopted to evaluate the anti-angiogenesis and irritancy potential of prepared nano *in situ* gel. Computational docking study carried out using glide module of Schrodinger software.

Results: The FT-IR study showed no interaction between the components. The drug-loaded nanoparticle showed particle size in the range of 369±5.3 to 410±3.5, followed by PDI 0.41±0.1 to 0.73±0.1, and ζ–Potential-13±2.3 to-9±3.4. The entrapment efficiency of nanoparticles was found in between the range of 72.35±1.4 to 87.22±1.1, followed by loading efficiency of 8.81±0.3 to 12.78±0.7. The FE-SEM studies resulted in an irregular pattern of aggregated particles. The spherical shape of the particles was confirmed through the HR-TEM study. The nano *in situ* gel exhibited pH in the range of 7.2±0.2 to 7.3±0.1 followed by a viscosity of 325.2±8.7 to 498.7±5.8 mPa. s. CAM assays revealed the safety and anti-angiogenesis activity of the developed formulation. All different concentrations of *in situ* gels of bevacizumab showed a significant anti-angiogenic effect. The outcome of the molecular docking study revealed the well-binding capacity of bevacizumab with vascular endothelial growth factor (-7.325) and human serum albumin (-5.620) residues.

Conclusion: The above outcomes improved our perception regarding the anti-angiogenic activity and safety of nano-*in situ* gels of bevacizumab. Overall, these findings denoted that implementing the current idea in the therapy of ocular angiogenesis might be a promising platform for better treatment.

Keywords: Nano *in situ* gel, Bevacizumab, Anti-angiogenic, Docking analysis, Ocular angiogenesis

INTRODUCTION

Angiogenesis is the growth of new blood vessels from the pre-existing vasculature [1]. Sufficient nutrients and oxygen will be supplied to the tumor cells mainly through angiogenesis. Hence, it divides and invades other healthy cells [2]. According to a recent report, globally, visual dysfunction is a significant problem in the aging population [3]. A research team analyzed global causes of blindness and distance vision impairment in those 50 y and older. The spectrum of disease includes cataracts followed by glaucoma, under-corrected refractive error, age-related macular degeneration (dry or wet), diabetic retinopathy (proliferative or non-proliferative), etc. [4]. Hypoxia is the leading cause of the uncontrolled proliferation of cells. It leads to the expression of vascular endothelial growth factor (VEGF), which can induce permeability and promote the mitosis of vascular endothelial cells [5, 6]. VEGF has been recognized as the lead factor responsible for ocular angiogenesis [7, 8].

Human serum albumin (HSA) is the protein most widely used in the targeted drug delivery system due to its high potential to load various drugs and deliver them to a specific site [9]. The drug bevacizumab (BVZ) has been extensively used off-label by physicians in treating ocular angiogenesis; it falls under the biological category of monoclonal antibodies [10]. Pharmacodynamically it is an antineoplastic agent that binds to VEGF and obstructs the interaction with its receptor on the endothelial cell surface, thereby inhibiting tumor cell activation, proliferation, and further angiogenesis, in response retardation of metastatic disease progression occurs [11, 12]. Injections of anti-VEGF drugs are in practice to treat ocular angiogenesis. However, repeated injections to the ocular region lead to complications like endophthalmitis, inflammation at the injection site, intraocular

pressure elevation, retinal detachment, etc. [13-15]. Therefore, it is necessary to design a novel drug delivery system to improve efficacy and minimize the drawbacks of the current dosage form. Recently, nanoparticles emerged as a novel technique in the pharmaceutical field that can deliver the drug to the specific targeted site effectively [16-18]. *In situ,* gel drug delivery is also a novel drug delivery system with dual advantages of liquid and gel [19, 20]. Considering the effective benefits of this system recently, research has been carried out on advanced techniques such as nanoparticles laden *in situ* gel [21, 22]. This drug delivery system aids sustained release action, enhanced drug retention time, improved bioavailability, specific site target, enhanced patient comfort, etc. Nanoparticles-laden *in situ* gel systems emerged as a widely acceptable and excellent drug delivery system in the ophthalmic sector. It seems to be the favoured therapy for patients due to the controlled release pattern of the drug, which ultimately reduces the dosing frequency and does not require the supervision of a medical practitioner to administer the medication. Hence, this novel drug delivery system enhanced patient compliance [23].

For the well-being of the animals, the committee named "Interagency Coordinating Committee on the Validation of Alternative Methods" (ICCVAM) introduced the Hen's Egg Test–Chorioallantoic Membrane (HET-CAM) assay. To promote the regulatory supervision and acceptance of testing method, which is new or revised, scientifically that ensures safety and product effectiveness [24]. The CAM model contains well-developed vasculature, i.e., complete tissue structure of arteries, veins, and capillaries [25]. Previous study outcomes revealed that the excellent correlation between ocular irritancy *in vivo* and response to injury is similar to rabbit conjunctiva [26]. Hence this can be an alternative to the Draize rabbit eye irritation test. Also, studies have reported that, because of its accessibility, dense capillary network system, and rapid growth, this was an excellent model and widely used assay for

in vivo angiogenesis studies [14, 27, 28]. Therefore, the present investigation is focused on elucidating the effect of nano-*in situ* gels of BVZ on the minute blood vessels of the HET-CAM membrane (mimicking the eye). The outcome of this investigation could provide a rationale for the utility of the nano-*in situ* gels of BVZ in the treatment of ocular angiogenesis. Other than formulation and evaluation of *in vitro* characteristics, it is essential to predict the binding affinities of the drug to the receptors or the other targets to achieve the efficacy of the designed formulation [29]. Hence, we conducted a molecular docking study to evaluate the ligand binding efficiency to the target and the ligand's inhibitory constant [30, 31]. Before *in vivo* assessment, the *in vitro* studies play a vital role in unveiling their efficacy against ocular angiogenesis. Accordingly, the current research work concentrated on the basic evaluation of prepared nano-*in situ* gel for its safety and efficacy against angiogenesis as well as the molecular docking approach to elucidate the interaction between the drug molecule and a protein, mainly at the atomic level with its binding affinity towards the target. A positive response provides a road map to further research, which may overcome hurdles associated with the current therapy.

MATERIALS AND METHODS

Materials

Avastin (BVZ) was purchased from Roche Products (India) Pvt. Ltd. (Mumbai, India). HSA was purchased from INTAS Biopharmaceuticals Pvt. Ltd. (Gujarat, India). Carbopol 934 and HPMC E 15 LV were acquired from LOBA Chemie Pvt. Ltd. (Mumbai, India). All reagents were of analytical grade.

Methods

Desolvation process

Nanoparticles were designed by desolvation process with some modifications as reported in Redín *et al.* 2018. The 200 µl of BVZ solution (Avastin) was added to the aqueous solution containing 100 mg HSA. Using 1 M HCl, the pH was adjusted to 4.9 and incubated for 10 min. To the above mixture, 16 ml ethanol was added and continuously stirred. The resulting solution was freeze-dried [9].

Double emulsion solvent evaporation method

The nanoparticles (NPs) were designed by taking 200 µl of BVZ solution with 10 mg of tween-80. The prepared mixture was added to the HSA-bearing organic solution of ethyl acetate (1.5 ml) and dichloromethane (0.5 ml) with continuous stirring (500 rpm). By using an ice bath, the emulsion was probe sonicated. Then oil/water emulsion was transferred into PVA (1 %) solution and again sonicated. The resulting solution was continuously stirred at room temperature. BVZ-encapsulated HSA nanoparticles were collected through a centrifugation process, washed, and then dispersed in 4% w/w mannitol solution (12,000 rpm, 4 °C, 15 min) (REMI CPR-24 PLUS, Bangalore, India) [32, 33]. The compositions of nanoparticles for the double emulsion solvent evaporation method are listed in table 1.

Fourier transform infrared spectroscopy (FT-IR) study

The compatibility within the components was assessed to monitor the shift of peaks using an FT-IR spectrophotometer (Shimadzu, Japan). The prepared samples were kept below the probe and scanned between the wave number region 4000-400 cm^{-1} [34, 35].

Determination of particle size, polydispersity index (PDI), and ζ–potential

The prepared nanoparticle formulation was analyzed for mean particle size, ζ-potential, and PDI by dynamic light scattering (DLS) using an advanced computerized inspection system (Malvern Zetasizer Ver. 7.13, Malvern, UK) [36].

Table 1: Composition of BVZ encapsulated HSA nanoparticles

Formulation code	BVZ (mg)	HSA (mg)	Tween 80 (mg)	Ethyl acetate (ml)	Dichloromethane (ml)	Polyvinyl alcohol (ml)	Mannitol (ml)
NP 1	-	100	10	1.5	0.5	5	8
NP 2	5	100	10	1.5	0.5	5	8
NP 3	5	100	30	1.5	0.5	10	8
NP 4	5	100	50	1.5	0.5	15	8
NP 5	5	100	70	1.5	0.5	20	8

Morphological analysis of nanoparticles by field emission scanning electron microscopy (FE-SEM) and high-resolution transmission electron microscopy (HR-TEM)

A formulation drop was placed over the sample holder and analyzed for the surface morphology of the nanoparticles using an FE-SEM (∑IGMA Carl Zeiss, Germany) analyzer [32]. The HR-TEM (JEM-2100 TEM, JEOL, Tokyo, JAPAN) was used to analyze the shape and morphological distribution. Before analysis, the samples were probe sonicated, placed over the copper-coated mesh, dried, and studied [36].

Determination of pH

The pH was monitored using a calibrated digital pH meter (LAB MAN LMPH-10, Mumbai, India). The glass electrode was kept in contact with the surface of the formulation, equilibrated for 1 min, and the pH was recorded [37].

Entrapment efficiency (% EE) and loading efficiency (% LE) determination

To evaluate the % EE and % LE, the nanoformulation was centrifuged at 12,000 rpm for 15 min using a cooling centrifuge (REMI CPR 24 PLUS, Bangalore, India). The supernatant was diluted as necessary and detected [32, 38].

$$\%EE = \frac{\text{total employed BVZ (mg)} - \text{BVZ in supernatant(mg)}}{\text{total employed BVZ (mg)}} * 100$$

$$\%LE = \frac{\text{total employed BVZ (mg)} - \text{BVZ in supernatant(mg)}}{\text{Nanoparticle mass (mg)}} * 100$$

Development of nano-*in situ* gel of BVZ

In situ gel solution was formulated by dispersing the weighed amount of carbopol 934 in water and dissolved completely using a magnetic stirrer (700 rpm) (REMI, 2MLH Bengaluru, India). Then HPMC E 15 LV was added and allowed to hydrate overnight. Benzalkonium chloride (BZK) was added to the above solution with the same stirring speed. Finally, the prepared nanoparticles were dispersed in a sufficient amount of gel solution to obtain nano-*in situ* gel (NP-ISG) [39, 40]. The composition of NP-ISG is listed in table 2.

Determination of gel clarity, pH, and viscosity

The clarity of the *in situ* gel formulation was visually examined before and after gelation under white and black backgrounds. The digital pH meter (LAB MAN LMPH-10, Mumbai, India) was used to monitor the pH of the prepared formulation [41]. The developed formulation's viscosity was detected using rheometer spindle 4 at a low shear rate of 1.32 s-1 (Brookfield AMETEK®, USA Model: DV3TLV) [42].

Table 2: Composition of NP-ISG

Formulation code	Carbopol 934 (% w/v)	HPMC E 15 LV (% w/v)	Benzalkonium chloride (% w/v)
NP-ISG 1	0.1	0.1	0.01

| NP-ISG 2 | 0.2 | 0.2 | 0.01 |
| NP-ISG 3 | 0.3 | 0.2 | 0.01 |

Gelling capacity and time

An accurately measured 20 µl of the prepared formulation was added to 2 ml of freshly prepared simulated tear fluid (STF) in a vial, and the time taken for gelling was noted [43].

Ocular irritation test/ocular toxicity study by HET-CAM assay

Briefly, fertilized hen's eggs were chosen and collected on day zero. Before starting the experiment, each egg was candled separately to avoid nonviable or defective ones. They are divided into five groups containing three eggs in each. All the eggs were incubated under certain conditions (37±0.5 °C and 55±7 % RH) (ROTEK, Omni, X-72, Kerala, India) for 9 d

[44]. Gently eggs were rotated every 12 h, and defective eggs were discarded from the study on the ninth day. Fertilized eggs shell was opened and divided into various groups (G) G I: vehicle control (water), G II: negative control (0.9 % NaCl), G III and IV: positive control [0.1 M NaOH and 1 % of sodium dodecyl sulfate (SDS)]. G V was treated with the formulation. The quantity of 0.5 ml was taken in a micropipette, added directly to the CAM surface without any damage to the membrane, and left for 5 min. The scoring was given in table 3 and observed for vascular injury. The categorization of substances according to the irritancy potential is shown in table 4. The irritation score was calculated as the mean sum of individual scores from three replicate assays of the endpoints (0, 0.5, 2, and 5 min) [24, 45].

Table 3: Score table for HET-CAM assay

Effect	Score		
	0.5 min	2 min	5 min
Hyperaemia	5	3	1
Hemorrhage	7	5	3
Coagulation	9	7	5

Table 4: Categorization of substances according to the irritancy potential

Irritancy potential	Category
0-0.9	Non-irritant
1-4.9	Weak-irritant
5-8.9	Moderate irritant
9–21	Severe irritant

Anti-angiogenesis test

Twenty fertilized hen's eggs were collected on day zero and sanitized. Eggs were divided into four groups (G I, II, III, and IV) containing five eggs in each and incubated (ROTEK, Omni, X-72, Kerala, India) [46]. G I was assigned as control. G II, III, and IV were treated with 100, 500, and 1000 µg of BVZ-containing formulation. The eggshell was opened on the 9th day, and all procedures were carried out in the sterile area to avoid contamination; egg windows were covered using sterile parafilm. The next day sealed windows were unlocked and observed using a microscope (Almicro Steriozoom Trinocular microscope Bangalore, India). The prepared formulations were added again and incubated for additional two

days. Later any changes in the diameter and length of blood vessels were assessed associated with the reduction of CAM area. Mountains Map Premium 8 software was used to study parameters like the Abbott curve, 3D surface views, and irregularities [47, 48].

Molecular docking analysis

Docking database studies were conducted using the Glide module of Schrodinger software (Schrodinger 2020-4, Ubuntu enterprise version 14.04 as an operating system). The structure of the target protein was retrieved from the RCSB protein data bank [49]. The required BVZ ligand was used as an input for the docking study and downloaded from PubChem databases. To build the ligand structures, chem sketch software was used and then subjected to the LigPrep module of the Schrodinger suite. [50, 51]. The protein data library revealed receptors with co-crystalline ligands such as PDB ID: 2BXB, 4AG8. These proteins were created using the protein preparation wizard module Schrodinger suite 2021-4. The protein crystal structures were produced with the help of a protein preparation wizard, and a co-crystallized ligand was encased within it. In our study, the Xtra precision (XP) docking model was used to predict the binding affinities of the target to ligand, ligand efficiency, and inhibitory ligand constant to the target [52-55].

Table 5: List of FT-IR peaks with characteristic functional groups

Sample	Characteristic peaks wave number (cm-1)	Characteristic functional group
	3270	Intense, broad O-H stretch
	2359	Strong O=C=O stretch
BVZ	1637	Amide I
	989	C=C bend
	658	CH=CH stretch
	3289	Intense, broad O-H stretch
HSA	1614	Amide I
	1535	Amide II
	3016	Intense, broad O-H stretch
	2936	Medium C-H stretching
Carbopol	2359	Strong O=C=O stretch
	1165	Strong C-O stretch
	798	Strong CH=CH bend
	668	CH=CH stretch
	3449	Medium N-H stretch
HPMC	2908	Medium C-H stretch
	1400-1300	Medium C-H bend
	944	C=C bend
	3270	Intense, broad O-H stretch
	2360	Strong O=C=O stretch
Formulation	1614	Amide I

| 1165 | Strong C-O stretch |
| 944 | C=C bending |

RESULTS AND DISCUSSION

FT-IR study

In the spectrum of BVZ, characteristic peaks occurred at 3279 cm^{-1}(O-H stretch), and this broadband may be due to the presence of hydroxyl groups. The peak at 1635 cm^{-1} confirmed the presence of the amide group. The stretching vibration of the CH=CH group was detected at 668 cm^{-1}. Similar findings were reported earlier by Zhang *et al.* 2018. In the FT-IR spectrum of HSA, sharp peaks were observed at 1641 cm^{-1} for the amide I. This band was mainly associated with the C=O stretch. The amide II group resulted 1545 cm^{-1} primarily from the N-H bending and C-N stretching vibration. Amides I and II are crucial bands in the protein structure spectrum.

These principal peaks for HSA were reported by Bummer in 1996. The absorption peak of carbopol 934 was observed at 3016 cm^{-1}. The peaks at 2936 and 798 cm^{-1} are recognized as the stretching vibrations of strong O=C=O and bending vibrations of CH=CH groups [56]. The HPMC E 15 LV spectrum displayed characteristic peaks at 3449 cm^{-1} recognized as medium stretching vibrations of N-H groups. The broader peak at the 1400-1300 cm^{-1} region was identified due to the medium bending vibrations of C-H groups [57]. The formulation spectra resulted in the same intensity peaks that confirmed no interactions between BVZ and the other excipients. This denoted the formulation was compatible. FT-IR spectra images depicted in fig. 1 and table 5 represent the list of peaks with distinct functional groups.
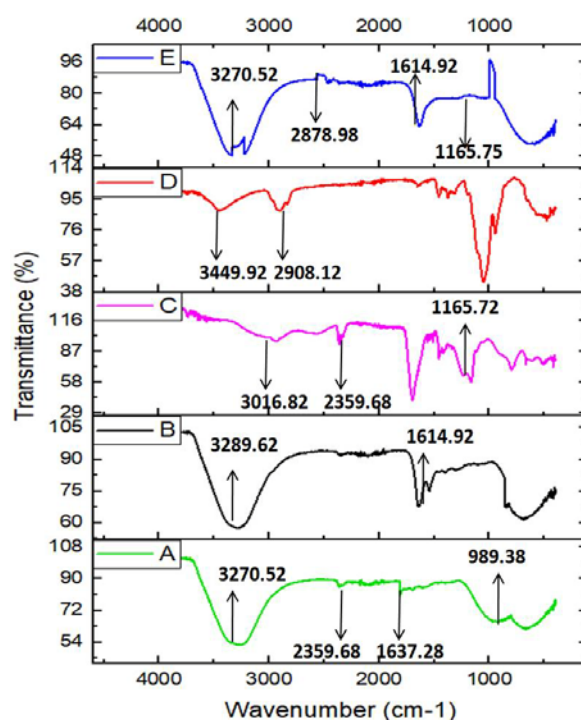

Fig. 1: FT-IR spectrum of (A) BVZ, (B) HSA, (C) Carbopol, (D) HPMC, (E) Formulation

Particle size, PDI, and ζ–potential determination

The DLS results revealed the obtained nanoparticles by the desolvation process showed significantly higher mean particle size and less entrapment efficiency than the double emulsion solvent evaporation method (table 6). Literature reported that nanoparticle prepared by the desolvation process leads to less mean particle size by cross-linking with the glutaraldehyde. But the use of glutaraldehyde is an issue due to its potential toxicity [9]. Considering all these points, we finalized the double emulsion solvent evaporation method for the formulation of nanoparticles. The placebo and drug-loaded nanoparticles were prepared and evaluated for characteristics like mean particle size, ζ–potential, and PDI. The mean particle size in placebo nanoparticles was 40±5.62 nm; for drug-loaded nanoparticles, it was 369±5.3 to 410±3.5 nm. The large size of particles was observed with drug-loaded nanoparticles than with placebo nanoparticles. The nanoparticle characterization results revealed that the surfactant concentration affects the particle size. Because when the surfactant concentration was high, a gradually enhanced particle size was observed, and the NP2 formulation code showed less particle size than the other formulations [32]. Literature reported that particle size greater than 10 μm might lead to irritation in the eye [57]. Hence,

obtained nanoparticles are in the acceptable range for ocular drug delivery. Fig. 2 displayed the particle size distribution of placebo and drug-loaded nanoformulation.

It is considered that the system is stable if the formulation shows ζ–potential in the+30 to-30 mV range. The fabricated placebo formulation showed ζ–potential of-14±2.03 mV, and gradually ζ–the potential was decreased in drug-loaded nanoparticles and lay in the range of-13±5.3 to-9±2.3. Even though the ζ–potential is negative, tween 80 as a surfactant will help to associate particles with the cornea. Additionally, the particles are further loaded in a pH-triggered system, which may help retain nanoparticles for an extended period in the ocular area [33, 57]. Fig. 3 depicts ζ–potential analysis of placebo and drug-loaded nanoparticles. PDI indicates the dispersion of particles in the formulation and laid in the range of 0.56±0.2 to 0.7±0.1. A lower PDI value indicates a monodispersity of the particles. Relatively uniform size particles were observed in the fabricated nanoparticle system. Previous findings revealed that a low PDI value indicated a narrow size range of particles within the formulation, which showed the mono distribution of the particles [58, 59]. Table 7 describes the results of particle size, PDI, and ζ–the potential of placebo and drug-loaded nanoparticles.

Table 6: Results of evaluated parameter for nanoparticles prepared by various techniques

Method	Particle size (nm)	PDI	ζ-Potential (mV)	% EE
Desolvation	449±0.7	0.67±0.2	-10±1.9	77.18±2.3
Double emulsion solvent evaporation	371±0.4	0.51±0.1	-14±2.5	83.17±3.5

All values were expressed as a mean±standard deviation (SD), n=3, *Double emulsion solvent evaporation method was chosen as a finalized procedure for the fabrication of nanoparticles.

Determination of pH, % EE and % LE

The pH of placebo nanoparticles was 7.1±0.2, and drug-loaded nanoparticles lay in the 6.6±0.3 to 6.3±0.2. The % EE of nanoparticles lay in the range of 87.22±1.1 to 72.35±1.4. The % LE of the nanoparticles was laid in the range of 12.78±0.7 to 8.81±0.3. The NP 2 formulation showed the highest percentage of entrapment and loading efficiency, and encapsulation was gradually decreased in NP 3, NP 4, and NP 5 formulations. As the surfactant concentration increased, a slight decrease in the entrapment of the drug was observed. It was confirmed that the surfactant concentration affects the drug encapsulation and loading efficiency [59]. All results are displayed in table 7.

Table 7: Results of evaluated parameters for unloaded and drug-loaded nanoparticles prepared by double emulsion solvent evaporation method

Evaluation parameter	NP 1	NP 2	NP 3	NP 4	NP 5
pH	7.1±0.2	6.6±0.3	6.2±0.5	6.1±0.4	6.3±0.2
Particle size (nm)	40±5.62	369±5.3	389±3.1	398±5.3	410±3.5
PDI	0.41±0.1	0.56±0.2	0.62±0.1	0.67±0.1	0.73±0.1
ζ-Potential (mV)	-14±2.03	-13±2.3	-11±5.3	-11±6.1	-9±3.4
EE (%)	NR	87.22±1.1	82.54±1.5	78.35±0.9	72.35±1.4
LE (%)	NR	12.78±0.7	11.28±0.6	10.51±0.5	8.81±0.3

All values were expressed as a mean±standard deviation (SD), n=3
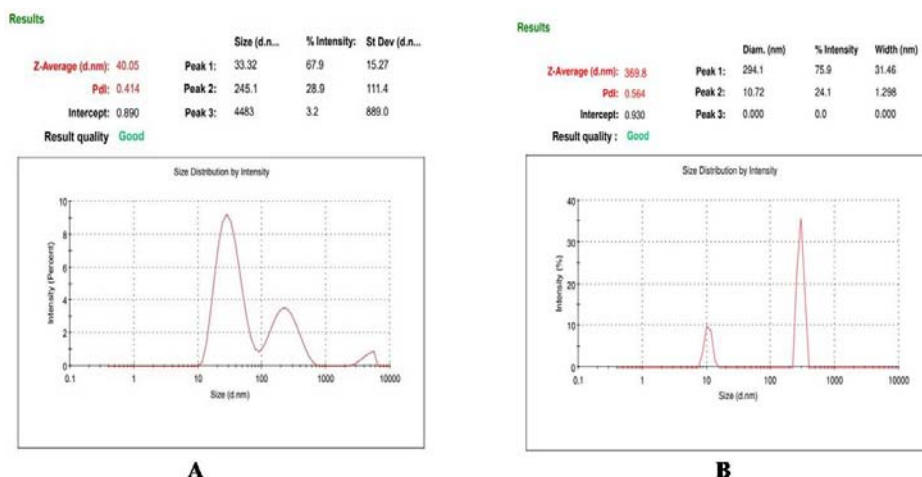
Fig. 2: Particle size distribution graph (A) Placebo nanoparticles (B) Drug-loaded nanoparticles
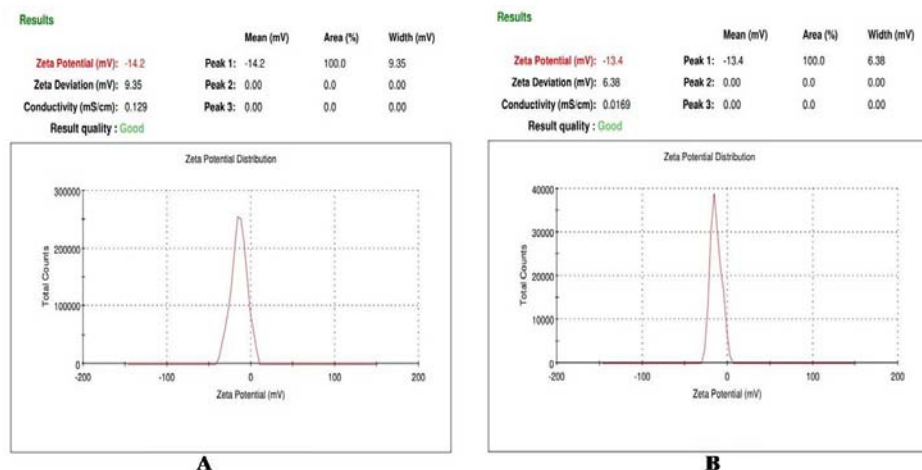
Fig. 3: Graph of zeta potential analysis (A) Placebo nanoparticles (B) Drug-loaded nanoparticles

Morphological analysis of nanoparticles by FE-SEM and HR-TEM

The FE-SEM images of nanoparticles are given in fig. 4. Simultaneously, irregular and aggregated particles were observed because of the lyophilized sample analysis [32]. The particles were aggregated and visualized as a mass of the particles. A uniform distribution of particles was observed; this might be due to the probe sonication process. The spherical shape of the particles was confirmed through the HR-TEM study (fig. 5). The dispersion of particles in the formulation was well observed in HR-TEM analysis, and the particle size results agreed with DLS measurements.
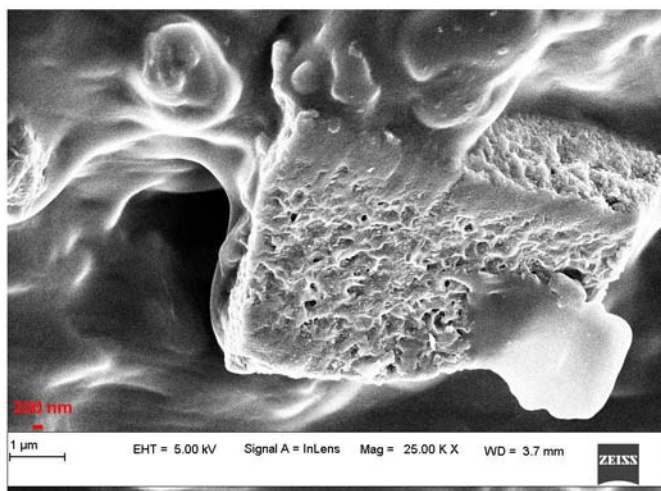

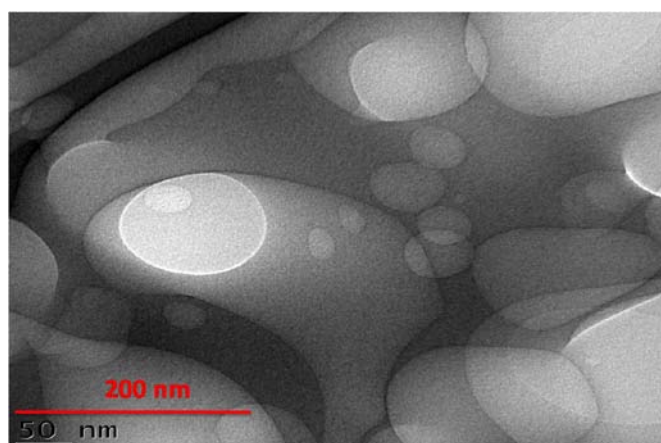**Fig. 4: FE-SEM image of nanoparticles**

Fig. 5: HR-TEM image of nanoparticles

Characterization of nano-*in situ* gel (NP-ISG)

In situ, gels can undergo a rapid sol-to-gel state by external stimuli like pH, temperature, ionic strength, etc. In this current investigation, the sol-to-gel transition occurs when there is a change in the pH. It may create irritation or a painful sensation if ophthalmic products have a pH far from tear fluid. The pH of the formulations was found in a suitable range between 5.8±0.4 to 6.1±0.3. After a transition from sol to gel, the pH ranged between 7.2±0.1 and 7.3±0.1. Literature reports that tears' buffering capacity could adjust the prepared product's pH to physiologic conditions. Therefore, the eye can tolerate the pH range of 3.5 to 8.5, and the pH of the current NP-ISG formulation was in an ideal range [60]. Clarity is an essential requirement for an ophthalmic dosage form, as it assures the patient compliance and acceptability of the formulation. The NP-ISG formulation was white and transparent. Viscosity determination is a prime factor that decides the retention time of formulation in the ocular area. The NP-ISG 1 showed less viscosity when compared with the other two formulations, which contain a high concentration of polymers. The current investigation viscosity of formulation lay in the 5.9±2.5 to 9.8±1.4 mPa. s for sol and 325.2±8.7 to 498.7±5.8 mPa. s for gel state. The viscosity of the formulation is directly proportional to the polymer concentration. When the concentration of the polymer increases, the viscosity of NP-ISG also increases. This is due to no dissociation at pH values below pKa due to the carboxyl group in the carbopol [61]. HPMC is a neutral polymer that hydrates polymer chains by forming hydrogen bonding [62]. Sol-to-gel transition is due to the ionization of functional groups in carbopol 934 at high pH, which increases electrostatic repulsion between the carboxyl group and polymeric network [37, 63]. The NP-ISG showed immediate gelation within 6 to 8s and remained for an extended period. In the current investigation, 0.3 % w/v carbopol 934 and 0.2 % w/v HPMC E 15 LV showed instant gelation within 6s and for an extended period. All the results are displayed in table 8.

HET-CAM assay

The HET-CAM model highly correlates with the vascularized mucosal tissue structure of the human eyes and reduces the unnecessary use of animals. This test is a simple, reproducible, rapid, and economical method to assess the ocular irritation study for prepared pharmaceutical formulations. The development process of chick embryo chorioallantoic membrane (d 1-9) is depicted in fig. 6. As shown in fig. 4 A. Initially, no blood vessels were seen; during embryonic growth, the rapid formation of blood vessels was observed. Embryonic development was initiated on day 3 and completed by day

9 [27]. The score table for the test formulations is displayed in table 9. The G I and G II groups were treated with vehicle and negative control, and the cumulative irritation score was 0 because no vascular damage was observed. The G III was treated with 0.1 M NaOH, and the cumulation irritation score was 13.6±4.50. The addition of 0.1 M NaOH led to the rupture of blood vessels initially, bleeding, and was followed by coagulation. G IV was treated with 1 % SDS, which led to vascular lysis and hemorrhage followed by coagulation, and the cumulative irritation score was 14.6±3.51. The cumulative irritation score of positive control chemicals used in the study showed that both fell

under the severe irritant category. The findings showed that 1 % SDS was more irritant than 0.1 M NaOH [64]. The last group (G V) was treated with NP-ISG formulation, no vascular damage was seen, and the cumulative irritation score was 0. Fig. 7. depicted CAM images for all treated groups. HET-CAM assay revealed that applying formulation vehicle (water), negative control (0.9 % NaCl), and formulation does not irritate the CAM membrane. Thus, the *ex vivo* ocular irritation/toxicity study guaranteed that NP-ISG formulation is non-irritant to the eye and safe at provided dosage after topical ocular administration [11, 24].

Table 8: Results of evaluated parameters for NP-ISG

Formulation code	Evaluation parameter						
	pH*		Clarity	Gelling	Gelling time (s)	Viscosity (mPa. s)*	
	Solution pH	gel pH		Capacity		At low pH	At high pH
NP-ISG 1	6.1±0.3	7.3±0.1	Transparent, White	++	15	5.9±2.5	325.2±8.7
NP-ISG 2	5.9±0.6	7.2±0.1	Transparent, White	+++	8	7.2±2.6	432.1±6.1
NP-ISG 3	5.8±0.4	7.2±0.2	Transparent, White	+++	6	9.8±1.4	498.7±5.8

+: gels after few min and dissolves within 45 min,++: gelation immediate, remains for few h,+++: gelation immediately remains for an extended period. *All values were expressed as a mean±SD. n=3
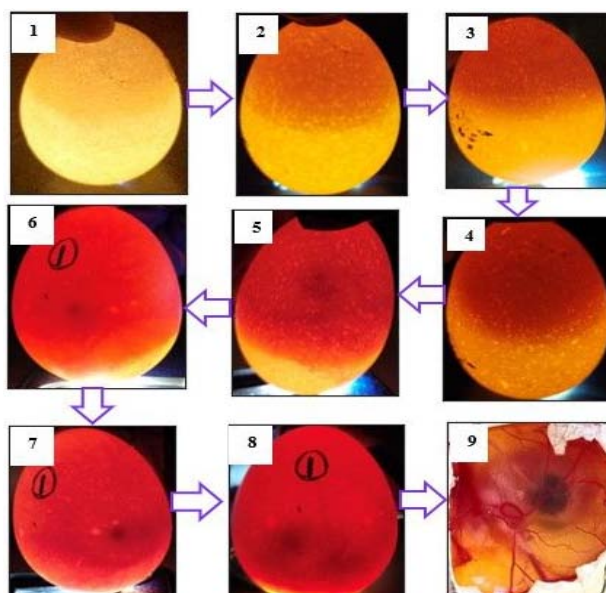

Fig. 6: Development process of chick embryo chorioallantoic membrane

Table 9: Score obtained in the HET-CAM test

| Group	Egg (E)	Scores									Mean score for 5 min
		Hyperaemia (A)			Hemorrhage (B)			Coagulation (C)			A+B+C/3
		Time (min)			Time (min)			Time (min)			
		0.5	2	5	0.5	2	5	0.5	2	5	
I Vehicle control (Water)	E 1	0	0	0	0	0	0	0	0	0	0
	E 2	0	0	0	0	0	0	0	0	0	
	E 3	0	0	0	0	0	0	0	0	0	
II Negative control (0.9 % NaCl)	E 1	0	0	0	0	0	0	0	0	0	0
	E 2	0	0	0	0	0	0	0	0	0	
	E 3	0	0	0	0	0	0	0	0	0	
III Positive control (0.1 M NaOH)	E 1	0	0	1	0	0	3	0	0	5	13.6±4.50
	E 2	0	0	1	0	5	0	0	7	5	
	E 3	0	0	1	0	5	3	0	0	5	
IV Positive control (1 % SDS)	E 1	0	3	0	0	5	0	0	7	0	14.6±3.51
	E 2	0	0	1	0	5	0	0	0	5	
	E 3	0	0	1	0	5	0	0	7	5	
V Formulation Treated	E 1	0	0	0	0	0	0	0	0	0	0
	E 2	0	0	0	0	0	0	0	0	0	
	E 3	0	0	0	0	0	0	0	0	0	

n=3
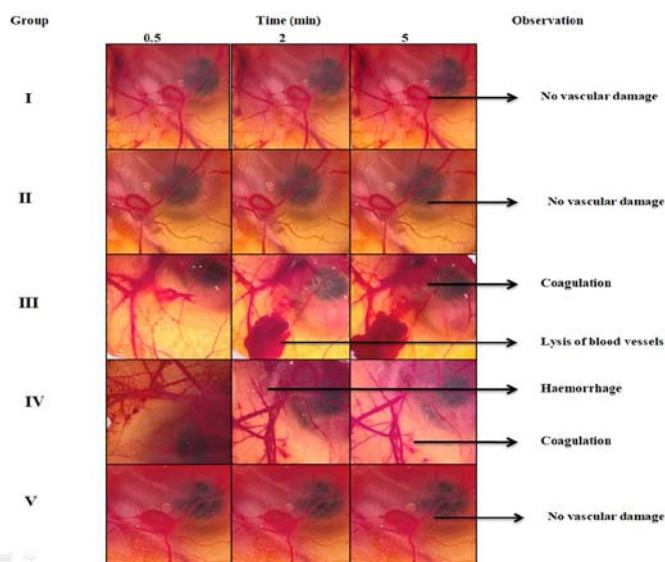
Fig. 7: Irritation study *ex vivo* (CAM images) GI: Vehicle control (water), G II: Negative control (0.9 % NaCl), G III: Positive control (0.1 M NaOH), G IV: Positive control (1 % SDS), G V: Formulation treated

Anti-angiogenesis test

This study assessed the effect of NP-ISG of BVZ on angiogenesis. In the CAM model, the vascular structural area originated from the main branch, which branched into primary, secondary, and tertiary. The formulation at different doses was applied to CAM chick embryos to study the anti-angiogenic effect at the macroscopic stage. The length and diameter of primary, secondary, and tertiary blood vessels were evaluated for 72 h. Fig. 8 showed a gradual reduction in the size and diameter of blood vessels in a treated group.

In contrast, the length and diameter of blood vessels gradually increased in the control group. The results showed diminishing primary and secondary blood vessels with the disappearance of tertiary blood vessels [65]. It concluded that the novel formulation inhibits the formation of new blood vessels. The NP-ISG formulation containing 1 mg of BVZ showed the amplest and strong anti-angiogenic effect. Blood vessel surface roughness was evaluated by Mountains Map Premium 8 software. The software assessed the fundamental parameters for 3D surface irregularities and given in table 10. Fig. 9 showed a 3D surface view for control and treated groups at 0 and 24 h. The surface roughness was higher in the control group, representing the neovascularisation, and significantly decreased in treated CAM. Fig. 10, the Abbott curve, describes the height of blood vessels in the control and treatment groups. A significant reduction in the size of the blood vessels in treated CAM revealed the anti-angiogenic activity of the developed formulation [66, 67]. Moreover, it was proven safe and effective against angiogenesis. However, deep insight research on this study will be worthwhile to continue systematically.

Table 10: Fundamental parameters for 3D surface irregularity

Parameter	Group I		Group II		Group III		Group IV	
	0 h	24 h	0 h	24 h	0 h	24 h	0 h	24 h
Arithmetic mean height (Sa)	19.40±1.2	23.80±1.5	20.01±1.4	16.92±2.1	24.15±2.5	10.07±2.9	25.14±3.4	9.86±3.9
Root mean squared height (Sq)	21.03±1.8	30.62±3.5	15.47±4.1	21.02±2.6	32.15±1.7	18.22±2.5	29.14±1.4	17.75±3.5
Maximum height (Sz)	197.54±6.5	213.3±7.5	218.01±8.5	211.14±7.9	208.30±5.2	142.0±6.4	195.42±8.9	135.3±5.4
Maximum valley depth (Sv)	74.21±2.5	85.54±6.4	58.10±1.8	54.98±2.2	74.38±3.4	54.90±3.6	72.15±4.1	54.12±1.7
Maximum peak height (Sp)	10.05±1.2	16.30±1.9	15.32±1.4	12.78±2.1	18.54±1.4	8.70±1.0	20.14±2.4	8.12±1.2

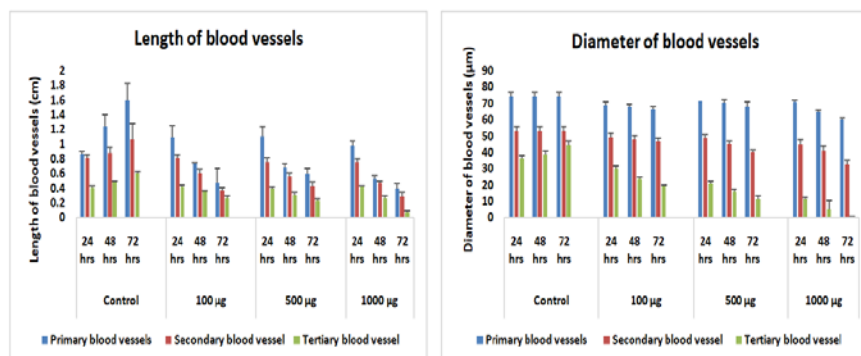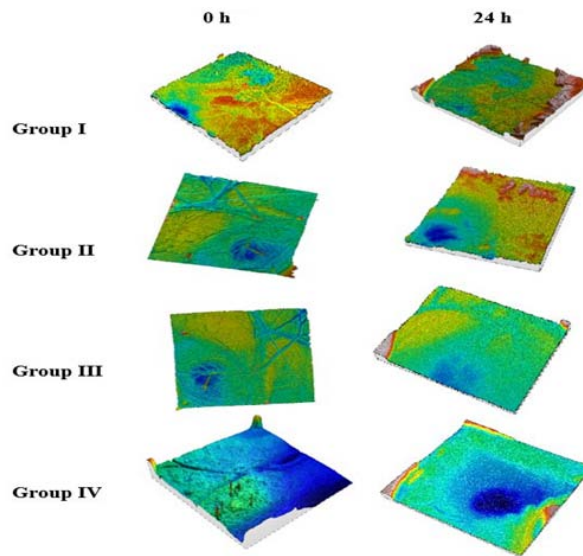*All values were expressed as a mean±SD. n=5

Fig. 8: Graphical representation of reduction of length and diameter of blood vessels in control and treated groups. All values were expressed as a mean±SD. n=5

Fig. 9: 3D surface view of HET-CAM area at 0 h and 24 h for control and treated groups [Group I: Control (not treated), Group II: 100 µg treated, Group III: 500 µg treated, Group IV: 1000 µg treated]
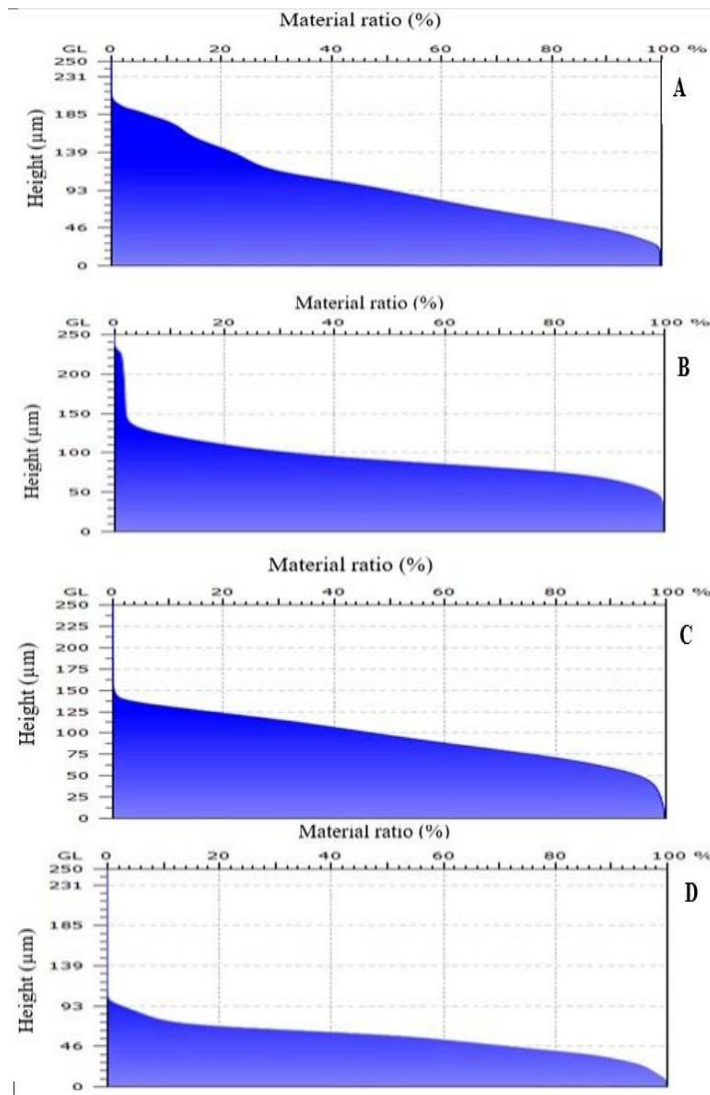
Fig. 10: Comparison of the height of blood vessels in the control and treatment group by Abbott curve. [A: Control (not treated), B: 100 µg treated, C: 500 µg treated, D: 1000 µg treated]

Molecular docking analysis

The binding capacity of drugs with protein is a crucial factor that affects bioavailability. Generally, when an active agent binds reversibly to the protein, which results in moderate binding strength, weak binding may lead to rapid metabolism and elimination. However, strong binding results in reduced drug concentration in the blood, ultimately required to produce the desired action. Therefore, a molecular docking study assessed the binding mode of the proposed compound BVZ with the VEGF and HSA. The molecular docking studies revealed a binding energy of-7.325 and-5.620 kcal/mol for VEGF and HSA, respectively (table 9). It has demonstrated well-countable binding affinity with the residues of VEGF receptors and HSA protein. The studies have reported that more negative binding energy indicates kinetic parameters regulating the thermodynamic features, *i.e.*, the formed complex's stability and the binding affinity between the protein and ligand. BVZ had the valuable docking score-5.620 with HSA (PDB ID:

2BXB) complex demonstrates that the contacts include *Tyr150, Glu153, Lyn199, Gln196, Phe211, Trp214, Ala215, Arg218, Leu219, Arg222, Leu238, Val241, Hie242, Arg257, Leu260, Ala261, Ile264, Ser287, Ile290, and Ala291*. Fig. 6 A shows their hydrogen bonding interaction with amino acid *Lyn 199* and π-π interaction with amino acid *Hie242*. The formation of intermolecular hydrogen bondsis responsible for more substantial complex formation and accurate docking results. BVZhad a valuable docking score of-7.325 with the VEGF(PDB ID: 4AG8)complex demonstrating that the contacts include *Leu840, Val848, Ala866, Val867, Lys868, Glu885, Leu889, Val899, Val914, Val916, Cys919, Cys1045,* and *Phe1047*. Fig. 6 B shows their ketonehydrogen binding interaction with amino acid *Thr1046.* This interaction mainly helps in stabilizing the target site's ligands and drug efficacy. Hydrophobic interaction with the residues of VEGF receptors and HSA proteins showed in table 11. Inhibition of the binding pocket of the VEGFR receptor has an essential effect on anti-cancer activities. BVZ compounds displayed excellent growth inhibitory activity against VEGF [68, 69].

Table 11: Results of docking score

S. No.	Ligand	Target name	Hydrophobic interactions	Glide docking XP score
1.	BVZ	HSA (PDB ID: 2BXB)	*Tyr150, Glu153, Lyn199, Gln196, Phe211, Trp214, Ala215, Arg218, Leu219, Arg222, Leu238, Val241, Hie242, Arg257, Leu260, Ala261, Ile264, Ser287, Ile290 and Ala291*	-5.620
		VEGF (PDB ID: 4AG8)	*Leu840,Val848, Ala866, Val867, Lys868, Glu885, Leu889, Val899, Val914, Val916, Cys919, Cys1045, and Phe1047*	-7.325

The docking scores were calculated using the Glide module of Schrodinger (Schrodinger 2020-4)
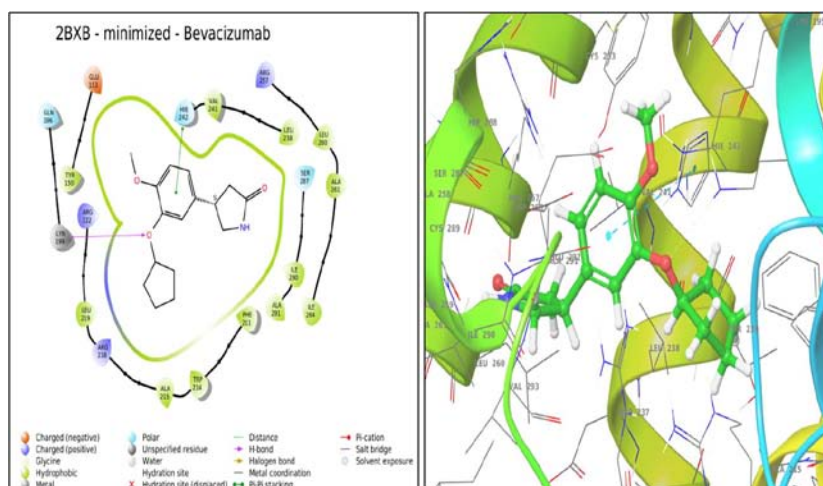

Fig. 11: 2D and 3D interactions of Amino-acid residue exhibited by the molecule BVZ in the active site of the target PDB: 2BXB
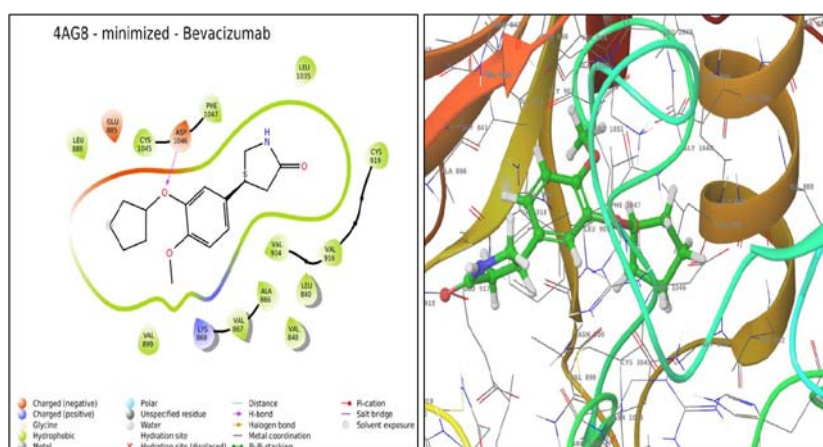

Fig. 12: 2D and 3Dinteractions of Amino-acid residue exhibited by the molecule BVZ in the active site of the target PDB: 4AG8

CONCLUSION

Clinically, intravitreal injections of BVZ are in practice for treating ocular angiogenesis. Repeated intravitreal injections are associated with several limitations, so here we worked with a novel formulation of BVZ for treating ocular angiogenesis. Before proceeding with *in vivo* studies, it is essential to evaluate the characteristics like safety and *in vitro* anti-angiogenesis effect. Molecular docking was performed to investigate the binding mode of the proposed compound BVZ with the VEGF and HSA. Therefore, in the present study, we sought to investigate the anti-angiogenic and irritancy potential of nano-*in situ* gels of BVZ using the HET-CAM assay. The HET-CAM model uses the chicken placenta, which mimics the ophthalmic situation *in vivo* with a well-developed vascularization structure. Docking analysis indicated that BVZ has a well-countable binding affinity with the residues of VEGF receptors and HSA protein. The present investigation revealed that the current formulation is safe and a promising treatment approach against angiogenesis. The novel technique designed in this paper offers the non-irritancy potential and effective anti-angiogenesis activity with a reduced dosage schedule, which may improve patient compliance with this new treatment approach. Overall, applying this approach to treat ocular angiogenesis as a novel drug delivery system promises further opportunities for the future.

STATEMENT OF HUMAN AND ANIMAL RIGHTS

This article does not contain any studies with human and animal subjects performed by any authors.

ABBREVIATION

HET CAM assay: Hen's egg test–chorioallantoic membrane assay; VEGF: Vascular endothelial growth factor; BVZ: Bevacizumab; ICCVAM: Interagency Coordinating Committee on the Validation of Alternative Methods; HSA: Human Serum Albumin; PVA: Poly (vinyl alcohol); FT-IR: Fourier transform infrared Spectroscopy; DLS: Dynamic Light Scattering; PDI: Polydispersity index; ZP: Zeta potential; EE: Entrapment Efficiency; LE: Loading Efficiency; HPMC: Hydroxypropyl Methyl Cellulose; BZK: Benzalkonium Chloride; NP-ISG: Nano *in situ* gel; STF: Simulated Tear Fluid; NaCl: Sodium Chloride; NaOH: Sodium hydroxide; SDS: Sodium dodecyl sulfate.

AUTHORS CONTRIBUTIONS

Soumya Narayana: Substantially contributed to protocol development, experimentation, data analysis, original manuscript design, and editing. Mohammed Gulzar Ahmed: Investigation, manuscript review, and editing. Arfa Nasrine: Manuscript review and editing. All authors have read and approved the manuscript.

CONFLICT OF INTERESTS

The authors declare that they have no conflict of interest.

REFERENCES

1. Pories SE, Wulf GM. Evidence for the role of bevacizumab in the treatment of advanced metastatic breast cancer: a review. Breast Cancer (Dove Med Press). 2010 Jun 21;2:37-44. doi: 10.2147/bctt.s6511. PMID 24367165, PMCID PMC3846523.
2. Yoo SY, Kwon SM. Angiogenesis and its therapeutic opportunities. Mediators Inflamm. 2013;2013:127170. doi: 10.1155/2013/127170, PMID 23983401, PMCID PMC3745966.
3. Steinmetz JD, Bourne RRA, Briant PS, Flaxman SR, Taylor HRB, Jonas JB. Causes of blindness and vision impairment in 2020 and trends over 30 years, and prevalence of avoidable blindness in relation to VISION 2020: the Right to Sight: an analysis for the Global Burden of Disease Study. Lancet Glob Heal. 2021;9(2):e144-60. doi: 10.1016/S2214-109X(20)30489-7.
4. Flaxman SR, Bourne RRA, Resnikoff S, Ackland P, Braithwaite T, Cicinelli MV. Global causes of blindness and distance vision impairment 1990-2020: a systematic review and meta-analysis. Lancet Glob Health. 2017 Dec;5(12):e1221-34. doi: 10.1016/S2214-109X(17)30393-5, PMID 29032195.
5. Michiels C. Physiological and pathological responses to hypoxia. Am J Pathol. 2004 Jun;164(6):1875-82. doi: 10.1016/S0002-9440(10)63747-9, PMID 15161623, PMCID PMC1615763.
6. Ferrara N. Role of vascular endothelial growth factor in the regulation of angiogenesis. Kidney Int. 1999 Sep;56(3):794-814. doi: 10.1046/j.1523-1755.1999.00610.x. PMID 10469350.
7. Siemerink MJ, Augustin AJ, Schlingemann RO. Mechanisms of ocular angiogenesis and its molecular mediators. Dev Ophthalmol. 2010;46:4-20. doi: 10.1159/000320006, PMID 20703029.
8. Narayana S, Ahmed MG, Gowda BHJ, Shetty PK, Nasrine A, Thriveni M. Recent advances in ocular drug delivery systems and targeting VEGF receptors for management of ocular angiogenesis: a comprehensive review. Futur J Pharm Sci. 2021;7(1):1-21.
9. Luis de Redin I, Boiero C, Martinez Oharriz MC, Agueros M, Ramos R, Penuelas I. Human serum albumin nanoparticles for ocular delivery of bevacizumab. Int J Pharm. 2018 Apr 25;541(1-2):214-23. doi: 10.1016/j.ijpharm.2018.02.003. PMID 29481946.
10. Colangelo AM, Bianco MR, Vitagliano L, Cavaliere C, Cirillo G, De Gioia L. A new nerve growth factor-mimetic peptide active on neuropathic pain in rats. J Neurosci. 2008 Mar 12;28(11):2698-709. doi: 10.1523/JNEUROSCI.5201-07.2008, PMID 18337399, PMCID PMC6670672.
11. Cao Y. Angiogenesis modulates adipogenesis and obesity. J Clin Invest. 2007 Sep;117(9):2362-8. doi: 10.1172/JCI32239, PMID 17786229, PMCID PMC1963348.
12. Ribatti D, Urbinati C, Nico B, Rusnati M, Roncali L, Presta M. Endogenous basic fibroblast growth factor is implicated in the vascularization of the chick embryo chorioallantoic membrane. Dev Biol. 1995 Jul;170(1):39-49. doi: 10.1006/dbio.1995.1193, PMID 7601314.
13. Falavarjani KG, Nguyen QD. Adverse events and complications associated with intravitreal injection of anti-VEGF agents: a review of literature. Eye (Lond). 2013 Jul;27(7):787-94. doi: 10.1038/eye.2013.107, PMID 23722722, PMCID PMC3709385.
14. Nguyen M, Shing Y, Folkman J. Quantitation of angiogenesis and antiangiogenesis in the chick embryo chorioallantoic membrane. Microvasc Res. 1994 Jan;47(1):31-40. doi: 10.1006/mvre.1994.1003, PMID 7517489.
15. Narayana S, Gulzar Ahmed M, Nasrine A. Effect of nano-encapsulation using human serum albumin on anti-angiogenesis activity of bevacizumab to target corneal neovascularization: development, optimization and *in vitro* assessment. Mater Today Proc. 2022;68:93-104. doi: 10.1016/j.matpr.2022.06.179.
16. Reimondez Troitino S, Csaba N, Alonso MJ, de la Fuente M. Nanotherapies for the treatment of ocular diseases. Eur J Pharm Biopharm. 2015 Sep;95(B):279-93. doi: 10.1016/j.ejpb.2015.02.019. PMID 25725262.
17. Hani U, Osmani RAM, Yasmin S, Gowda BHJ, Ather H, Ansari MY. Novel drug delivery systems as an emerging platform for stomach cancer therapy. Pharmaceutics. 2022 Jul 29;14(8):14(8):1576. doi: 10.3390/pharmaceutics14081576, PMID 36015202.
18. Gowda BHJ, Ahmed MG, Chinnam S, Paul K, Ashrafuzzaman M, Chavali M. Current trends in bio-waste mediated metal/metal oxide nanoparticles for drug delivery. J Drug Deliv Sci Technol. 2022;71(Mar):103305. doi: 10.1016/j.jddst.2022.103305.
19. Ambikar RB, Bhosale AV. Original article development and characterization of diclofenac sodium loaded eudragit rs100 polymeric microsponge incorporated into in situ gel for ophthalmic drug delivery system. Int J Pharm Pharm Sci. 2021;13(9):63-9.

20. Dholakia M, Dave R, Thakkar V, Rana H, Gohel M, Patel N. Newer ophthalmic in situ gel of moxifloxacin hydrochloride: optimization using box Behnken statistical design. Int J Pharm Pharm Sci. 2018;10(12):5-13. doi: 10.22159/ijpps.2018v10i12.26979.

21. Jain N, Verma A. Preformulation studies of pilocarpine hydrochloride as niosomal gels for ocular drug delivery. Asian J Pharm Clin Res. 2020;13(6):149-55. doi: 10.22159/ajpcr.2020.v13i6.37523.

22. Paulsamy M, Ponnusamy C, Palanisami M, Nackeeran G, Paramasivam S, Sugumaran A. Nepafenac loaded silica nanoparticles dispersed in-situ gel systems: development and characterization. Int J Biol Macromol. 2018 Apr 15;110:336-45. doi: 10.1016/j.ijbiomac.2018.01.123. PMID 29408555.

23. Kumar D, Jain N, Gulati N, Nagaich U. Nanoparticles laden in situ gelling system for ocular drug targeting. J Adv Pharm Technol Res. 2013 Jan;4(1):9-17. doi: 10.4103/2231-4040.107495, PMID 23662277, PMCID PMC3645361.

24. Kandarova H, Letasiova S. Alternative methods in toxicology: pre-validated and validated methods. Interdiscip Toxicol. 2011 Sep;4(3):107-13. doi: 10.2478/v10102-011-0018-6, PMID 22058651, PMCID PMC3203912.

25. Cazedey ECL, Carvalho FC, Fiorentino FAM, Gremiao MPD, Salgado HRN. Corrositex®, BCOP and HET-CAM as alternative methods to animal experimentation. Braz J Pharm Sci. 2009;45(4):759-66. doi: 10.1590/S1984-82502009000400021.

26. Saurabh SS, Rathore KS, Ghosh S. Formulation and evaluation of cetirizine hydrochloride ph trigged in-situ ocular gel. Int J Appl Pharm. 2023;15(2):106-16.

27. Nowak Sliwinska P, Segura T, Iruela Arispe ML. The chicken chorioallantoic membrane model in biology, medicine and bioengineering. Angiogenesis. 2014 Oct;17(4):779-804. doi: 10.1007/s10456-014-9440-7, PMID 25138280, PMCID PMC4583126.

28. Kundekova B, Macajova M, Meta M, Cavarga I, Bilcik B. Chorioallantoic membrane models of various avian species: differences and applications. Biology (Basel). 2021 Apr 6;10(4):301. doi: 10.3390/biology10040301, PMID 33917385, PMCID PMC8067367.

29. Shaikh MS, Kale MA. Formulation and molecular docking simulation study of luliconazole nanosuspension–based nanogel for transdermal drug delivery using modified polymer. Mater Today Chem. 2020;18:100364. doi: 10.1016/j.mtchem.2020.100364.

30. Rani KC, Parfati N, Aryani NLD, Winantari AN, Fitriani EW, Pradana AT. Development, evaluation, and molecular docking of oral dissolving film of atenolol. Pharmaceutics. 2021 Oct 19;13(10):1727. doi: 10.3390/pharmaceutics13101727, PMID 34684021, PMCID PMC8537485.

31. Mohamed JMM, Alqahtani A, Kumar TVA, Fatease AA, Alqahtani T, Krishnaraju V. Superfast synthesis of stabilized silver nanoparticles using aqueous allium sativum (garlic) extract and isoniazid hydrazide conjugates: molecular docking and *in vitro* characterizations. Molecules. 2021 Dec 24;27(1):110. doi: 10.3390/molecules27010110, PMID 35011342, PMCID PMC8746848.

32. Zhang XP, Sun JG, Yao J, Shan K, Liu BH, Yao MD. Effect of nanoencapsulation using poly (lactide-co-glycolide) (PLGA) on anti-angiogenic activity of bevacizumab for ocular angiogenesis therapy. Biomed Pharmacother. 2018 Nov;107:1056-63. doi: 10.1016/j.biopha.2018.08.092. PMID 30257317.

33. Tao W, Zeng X, Liu T, Wang Z, Xiong Q, Ouyang C. Docetaxel-loaded nanoparticles based on star-shaped mannitol-core PLGA-TPGS diblock copolymer for breast cancer therapy. Acta Biomater. 2013 Nov;9(11):8910-20. doi: 10.1016/j.actbio.2013.06.034. PMID 23816645.

34. Varshochian R, Riazi Esfahani M, Jeddi Tehrani M, Mahmoudi AR, Aghazadeh S, Mahbod M. Albuminated PLGA nanoparticles containing bevacizumab intended for ocular neovascularization treatment. J Biomed Mater Res A. 2015 Oct;103(10):3148-56. doi: 10.1002/jbm.a.35446. PMID 25773970.

35. Bummer PM. An FTRI study of the structure of human serum albumin adsorbed to polysulfone. International Journal of Pharmaceutics. 1996;132(1-2):143-51. doi: 10.1016/0378-5173(95)04344-6.

36. Tarhini M, Benlyamani I, Hamdani S, Agusti G, Fessi H, Greige Gerges H. Protein-based nanoparticle preparation via nanoprecipitation method. Materials (Basel). 2018 Mar 7;11(3):394. doi: 10.3390/ma11030394, PMID 29518919, PMCID PMC5872973.

37. Singh J, Chhabra G, Pathak K. Development of acetazolamide-loaded, pH-triggered polymeric nanoparticulate in situ gel for sustained ocular delivery: *in vitro*. Ex vivo evaluation and pharmacodynamic study. Drug Dev Ind Pharm. 2014;40(9):1223-32. doi: 10.3109/03639045.2013.814061, PMID 23837522.

38. Upadhayay P, Kumar M, Pathak K. Norfloxacin loaded pH triggered nanoparticulate in-situ gel for extraocular bacterial infections: optimization, ocular irritancy and corneal toxicity. Iran J Pharm Res. 2016;15(1):3-22. PMID 27610144, PMCID PMC4986130.

39. Gupta H, Aqil M, Khar RK, Ali A, Bhatnagar A, Mittal G. Sparfloxacin-loaded PLGA nanoparticles for sustained ocular drug delivery. Nanomedicine. 2010 Apr;6(2):324-33. doi: 10.1016/j.nano.2009.10.004. PMID 19857606.

40. Pathak MK, Chhabra G, Pathak K. Design and development of a novel pH triggered nanoemulsified in-situ ophthalmic gel of fluconazole: ex-vivo transcorneal permeation, corneal toxicity and irritation testing. Drug Dev Ind Pharm. 2013 May;39(5):780-90. doi: 10.3109/03639045.2012.707203, PMID 22873799.

41. Wadhwa K, Sharma C, Goswami M, Thakur N. Formulation and evaluation of pH triggered *in-situ* ocular gel of ofloxacin. IJPSR. 2019;10:4507-12. doi: 10.13040/IJPSR.0975-8232.10(10).4507-12.

42. Kurniawansyah IS, Rusdiana T, Sopyan I, Ramoko H, Wahab HA, Subarnas A. In situ ophthalmic gel forming systems of poloxamer 407 and hydroxypropyl methyl cellulose mixtures for sustained ocular delivery of chloramphenicole: optimization study by factorial design. Heliyon. 2020;6(11):e05365. doi: 10.1016/j.heliyon.2020.e05365. PMID 33251348.

43. Nagai N, Minami M, Deguchi S, Otake H, Sasaki H, Yamamoto N. An in situ gelling system based on methylcellulose and tranilast solid nanoparticles enhances ocular residence time and drug absorption into the cornea and conjunctiva. Front Bioeng Biotechnol. 2020;8:764. doi: 10.3389/fbioe.2020.00764, PMID 32733870.

44. Prinsen MK, Hendriksen CFM, Krul CAM, Woutersen RA. The isolated chicken eye test to replace the draize test in rabbits. Regul Toxicol Pharmacol. 2017 Apr;85:132-49. doi: 10.1016/j.yrtph.2017.01.009. PMID 28192172.

45. Budai P, Lehel J, Tavaszi J, Kormos E. HET-CAM test for determining the possible eye irritancy of pesticides. Acta Vet Hung. 2010 Sep;58(3):369-77. doi: 10.1556/AVet.58.2010.3.9, PMID 20713327.

46. Kıyan HT, Demirci B, Başer KH, Demirci F. The *in vivo* evaluation of anti-angiogenic effects of hypericum essential oils using the chorioallantoic membrane assay. Pharm Biol. 2014 Jan;52(1):44-50. doi: 10.3109/13880209.2013.810647, PMID 24044783.

47. Khan GJ, Omer MO, Ashraf M, Rehman HU, Khan ZU. Effect of punica granatum (pomegranate) fruit extract on angiogenesis. J Appl Pharm. 2013;4(2):764-80.

48. Katrancioglu N, Karahan O, Kilic AT, Altun A, Katrancioglu O, Polat ZA. The antiangiogenic effects of levosimendan in a CAM assay. Microvasc Res. 2012 May;83(3):263-6. doi: 10.1016/j.mvr.2012.01.002. PMID 22285653.

49. Pandey RK, Kumbhar BV, Srivastava S, Malik R, Sundar S, Kunwar A. Febrifugine analogues as Leishmania donovani trypanothione reductase inhibitors: binding energy analysis assisted by molecular docking, ADMET and molecular dynamics simulation. J Biomol Struct Dyn. 2017 Jan;35(1):141-58. doi: 10.1080/07391102.2015.1135298, PMID 27043972.

50. Kumar A, Rathi E, Kini SG. E-pharmacophore modelling, virtual screening, molecular dynamics simulations and in-silico ADME analysis for identification of potential E6 inhibitors against cervical cancer. J Mol Struct. 2019;1189:299-306. doi: 10.1016/j.molstruc.2019.04.023.

51. Chowdhury KH, Chowdhury MR, Mahmud S, Tareq AM, Hanif NB, Banu N. Drug repurposing approach against novel

coronavirus disease (COVID-19) through virtual screening targeting SARS-CoV-2 main protease. Biology (Basel). 2020 Dec 23;10(1):2. doi: 10.3390/biology10010002, PMID 33374717, PMCID PMC7822464.

52. Prabhu S, Vijayakumar S, Manogar P, Maniam GP, Govindan N. Homology modeling and molecular docking studies on type II diabetes complications reduced PPARγ receptor with various ligand molecules. Biomed Pharmacother. 2017 Aug;92:528-35. doi: 10.1016/j.biopha.2017.05.077. PMID 28575810.

53. Umamaheswari A, Kumar MM, Pradhan D, Marisetty H. Docking studies towards exploring antiviral compounds against envelope protein of yellow fever virus. Interdiscip Sci. 2011;3(1):64-77. doi: 10.1007/s12539-011-0064-y, PMID 21369890.

54. Desai N, Mahto MK, Alekhya B, Naveen CR, Bhaskar M. Comparative docking studies of estrogen receptor inhibitors and their binding interaction analysis. Int J Pharm Sci Rev Res. 2012;16(9).

55. Garala K, Joshi P, Shah M, Ramkishan A, Patel J. Formulation and evaluation of periodontal in situ gel. Int J Pharm Investig. 2013 Jan;3(1):29-41. doi: 10.4103/2230-973X.108961, PMID 23799203, PMCID PMC3687234.

56. Sri KV, Rohini P, Reddy GK. Montelukast sodium oral thin films: formulation and *in vitro* evaluation. Asian J Pharm Clin Res. 2012;5:266-70.

57. Laddha UD, Kshirsagar SJ. Formulation of nanoparticles loaded in situ gel for treatment of dry eye disease: *in vitro*, ex vivo and *in vivo* evidences. J Drug Deliv Sci Technol. 2021 Feb 1;61:102112. doi: 10.1016/j.jddst.2020.102112.

58. Morsi N, Ibrahim M, Refai H, El Sorogy H. Nanoemulsion-based electrolyte triggered in situ gel for ocular delivery of acetazolamide. Eur J Pharm Sci. 2017 Jun 15;104:302-14. doi: 10.1016/j.ejps.2017.04.013. PMID 28433750.

59. Sousa F, Cruz A, Fonte P, Pinto IM, Neves Petersen MT, Sarmento B. A new paradigm for antiangiogenic therapy through controlled release of bevacizumab from PLGA nanoparticles. Sci Rep. 2017 Jun 16;7(1):3736, https://doi.org/10.1038/s41598-017-03959-4, PMID 28623267.

60. Ammar HO, Salama HA, Ghorab M, Mahmoud AA. Nanoemulsion as a potential ophthalmic delivery system for dorzolamide hydrochloride. AAPS PharmSciTech. 2009;10(3):808-19, https://doi.org/10.1208/s12249-009-9268-4, PMID 19536653.

61. Kute PR, Gondkar SB, Saudagar RB. Ophthalmic in-situ gel: an overview. WJJPS. 2015;4:549-68. doi: 10.22270/jddt.v9i1.2231.

62. Ford JL. Design and evaluation of hydroxypropyl methylcellulose matrix tablets for oral controlled release: a historical perspective. Hydrophilic Matrix Tablets for Oral. J Control Release. 2014:17-51. doi: 10.1007/978-1-4939-1519-4_2.

63. Singh SK, Verma PR, Razdan B. Glibenclamide-loaded self-nanoemulsifying drug delivery system: development and characterization. Drug Dev Ind Pharm.. 2010 Aug;36(8):933-45. doi: 10.3109/03639040903585143, PMID: 20184416.

64. Budai P, Kormos E, Buda I, Somody G, Lehel J. Comparative evaluation of HET-CAM and ICE methods for objective assessment of ocular irritation caused by selected pesticide products. Toxicol *In Vitro*. 2021;74:105-50. doi: 10.1016/j.tiv.2021.105150. PMID 33753176.

65. Hussain I, Omer MO, Ashraf M. Effect of diclofenac sodium angiogenesis using chorioallantoic membrane (cam) assay. Journal of Applied Pharmacy. 2011 Jun 27;3:320-30.

66. Bashir MF, Qadir MI. Effect of ginger extract on angiogenesis using CAM assay. Bangladesh J Pharmacol. 2017;12(3):348-53, doi: 10.3329/bjp.v12i3.32616.

67. Saleem U, Ahmad B, Ahmad M, Hussain K, Bukhari NI, Ashraf M. Evaluation of anti-angiogenic activity of latex and extracts of Euphorbia helioscopia using chorioallontoic membrane (CAM) assay. Int J Agric Biol. 2015 Apr 30;17(2).

68. Du X, Li Y, Xia YL, Ai SM, Liang J, Sang P. Insights into protein–ligand interactions: mechanisms, models, and methods. Int J Mol Sci. 2016;17(2):1-34. doi: 10.3390/ijms17020144, PMID 26821017.

69. Mukherjee S, Chatterjee G, Ghosh M, Das B, Majumder D. Efficacy and toxicity assessment of different antibody based antiangiogenic drugs by computational docking method. Advances in Bioinformatics. 2016:1-117053712, https://doi.org/10.1155/2016/7053712, PMID 27047544.

70. Chandrasekaran V, Ambati J, Ambati BK, Taylor EW. Molecular docking and analysis of interactions between vascular endothelial growth factor (VEGF) and SPARC protein. Journal of Molecular Graphics and Modelling. 2007 Nov 1;26(4):775-82, doi: 10.1016/j.jmgm.2007.05.001. PMID 17560152.